ACS APPLIED MATERIALS & INTERFACES

www.acsami.org

Research Article

Chiral Control of Carbon Dots via Surface Modification for Tuning the Enzymatic Activity of Glucose Oxidase

Mengling Zhang, Yurong Ma, Huibo Wang, Bo Wang, Yunjie Zhou, Yang Liu,* Mingwang Shao, Hui Huang,* Fang Lu,* and Zhenhui Kang*

Cite This: *ACS Appl. Mater. Interfaces* 2021, 13, 5877−5886

Read Online

ACCESS | Metrics & More | Article Recommendations | Supporting Information

ABSTRACT: Chiral carbon dots (CDs) integrated the advantages of achiral CDs and the unique chiral property, which expand the prospect of the biological applications of CDs. However, the structure control and the origin of chirality for chiral CDs remain unclear. Herein, chiral CDs were obtained by thermal polymerization of chiral amino acids and citric acid, and their handedness of chirality could be controlled by adjusting the reaction temperature, which leads to different kinds of surface modifications. With aliphatic amino acids as a chiral source, all of the CDs that reacted at different temperatures (90−200 °C) have the same handedness of the chiral source. But with aromatic amino acids as a chiral source, CDs with maintained or inversed handedness compared with the chiral source could be obtained by adjusting the reaction temperature. Below a temperature of 120 °C, the chiral source was modified with CDs by esterification and transferred the handedness of chirality; at high temperatures (above 150 °C), which mainly connected by amidation accompanying with the formation of rigid structure generated by the π conjugation between the aromatic nucleus of chiral source and the carbon core of CDs, caused the inversing of the chiral signal. Further, we investigated the chiral effects of CDs on the glucose oxidase activity for a highly sensitive electrochemical biosensor.

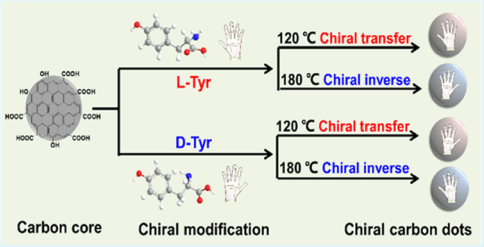

KEYWORDS: *carbon dots, handedness, chiral control, enzymatic activity, glucose oxidase*

1. INTRODUCTION

Chirality plays a crucial effect in chemical recognition and interactions between chemical and biological species, relating to many application fields including chiral recognition, chiral catalysis, and chiral bio-nanoscience.[1−3] Chiral nanostructures have shown great potential and a promising future for sensing,[4] cytotoxicity mediation and cell imaging,[5,6] asymmetric catalysis and enantiomeric separation,[2,7,8] circularly polarized light sources, and spintronics.[9−11] In 1998, Schaaff et al. first reported the chiral nanoparticles, stabilizing chiral glutathione to gold nanoclusters.[12] However, the study on the fabrication and properties of chiral nanostructures is still in its infancy. Four fabrication categories of chiral nanomaterials have been developed according to their origin of chirality: (1) the induced chirality by integrating chiral molecules (absorption or covalent conjugation) into a nanoparticle;[13,14] (2) the geometrical chirality by a template method;[15,16] (3) nanoparticles with the intrinsically chiral crystal lattice such as selenium and tellurium nanocrystals;[17,18] and (4) chiral nanomaterials fabricated by chiral driving force (such as circularly polarized light, electric field, and magnetic field).[19−22] A better and deep understanding on the structure and properties of the chiral nanostructures needs further systematic experimental and theoretical studies.

Carbon dots (CDs) stimulated great interests in many fields due to their unique fluorescent property, easy functionalization, and good biocompatibility.[23−25] Notably, chirality will give CDs more unique properties to enhance the prospect of their biological applications. Recently it has been demonstrated that the chirality of CDs had an impact on cytotoxicity,[26] cellular energy metabolism,[27] Golgi apparatus imaging,[28] antibiosis,[29] regulating plant growth, and tuning enzymatic activity.[30−32] The chiral CDs, reported so far, were obtained by pyrolysis,[29] microwave-assisted synthesis,[33] electrochemical method,[31,32] hydrothermal method, and chemical oxidation.[27,34,35] However, the origin of chirality and the structure control still remain unclear.

Herein, we reported that chiral CDs were prepared by thermal polymerization from citric acid and chiral amino acids, and the handedness of CDs can be regulated by adjusting the reaction temperature. With chiral tyrosine (Tyr) as a reagent, the chiral CDs could inherit the same circular dichroism absorption of the chiral material at 120 °C, whereas the chiral CDs with the inverted chiral signal could be obtained at higher temperature (above 150 °C). Further, for aliphatic amino acids

Received: December 10, 2020
Accepted: January 11, 2021
Published: January 22, 2021

(serine, glutamic acid, and so on), the handedness of CDs was transferred by a chiral source via surface modification. For aromatic amino acids (tyrosine, phenylalanine, and tryptophan), the chiral CDs could inherit the same circular dichroism signal of the chiral material at 120 °C, whereas the chiral CDs with the inverted circular dichroism signal could be obtained at 180 °C because of the rigid structure generated by an amide bond and the conjugation of π electron between the aromatic nucleus of amino acid and the carbon core. We further demonstrated that these chiral CDs are efficient substrate to enhance the glucose oxidase (GOx) activity for the design of a highly sensitive GOx-based direct electrochemical biosensor.

2. EXPERIMENTAL SECTION

2.1. Materials. The GOx and amino acids used in this work were purchased from Shanghai Aladdin Bio-Chem Technology Co. Ltd. Citric acid and a cellulose dialysis bag (500−1000 Da) were purchased from Shanghai Yuanye Biotechnology Co. Ltd. (S)-3-Amino-2-benzylpropanoic acid ((S)-ABPA) was purchased from WuXi AppTec Co. Ltd. A glucose oxidase enzyme-linked immunosorbent assay (ELISA) test kit was provided by Kejing Biological Technology Co. Ltd. All chemicals were used without any further purification.

2.2. Synthesis of Chiral CDs. Chiral CDs were obtained by a two-step method. Briefly, the citric acid powder (2.00 g) in a round-bottom flask was carbonized in an oil bath of 200 °C for 30 min, and the carbon core was obtained. Then, 1.20 g of the L-/D-Tyr powder was added into the round-bottom flask. The substances were mixed by a glass rod and treated with different temperatures (120/180 °C) for 30 min, respectively. During the reaction, the mixture turned orange and viscous, as a result of the connection of a carbon core and L-/D-Tyr. After 30 min, 20 mL of ultrapure water was added for dissolving the product. Finally, the crude product was subjected to filtration and dialysis (500−1000 Da) for further purification, and the orange colored chiral CDs were obtained. To study the effects of reaction parameters on the handedness of products, different reaction temperatures (90, 120, 150, 180, and 200 °C) and reaction times (15, 30, 60, and 90 min) were used in step 2.

2.3. Preparation of GOx-CDs Hybrids. The GOx powder (30.00 mg) was dissolved in 2 mL of 0.1 mol/L phosphate-buffered saline (PBS, pH = 7.2) first, and then an equal amount (2 mL) of 4.00 mg/mL chiral CDs (120-LTyr-CDs, 120-DTyr-CDs, 180-LTyr-CDs, and 180-DTyr-CDs) was added and these mixtures were incubated at 35 °C for 4 h. Finally, the GOx-CDs-1, GOx-CDs-2, GOx-CDs-3, and GOx-CDs-4 hybrids were obtained. These hybrids were stored at 4 °C before use.

2.4. Activity Assays of GOx-CDs Hybrids. The enzymatic activity of GOx and GOx-CDs hybrids were measured by a glucose oxidase ELISA test kit. In the preparation of GOx-CDs hybrids, the same concentration (7.5 mg/mL) of free GOx was used and incubated at 35 °C for 4 h. To ensure the enzymatic activity of samples was in the range of the standard curve of the test kit, the GOx and GOx-CDs hybrids were diluted 20 times before detection.

2.5. Glucose Detection with a GOx-CDs Enzyme Electrode. A glassy carbon electrode (GCE) was polished by 50 nm alumina slurry and washed by deionized water. Then, the pretreatment, cyclic voltammetric (CV) scanning in 0.5 mol/L H_2SO_4 for 30 min (−1 to 1 V with a scan rate of 10 mV/s), was performed to activate the surface of GCE. After washing with deionized water and drying, the GCE was cast by 10 μL of a GOx-CDs hybrid, and the GOx-CDs-modified GCE was dried in the shade at 4 °C. For avoiding the spilling of the sample, 10 μL of a 0.5% Nafion water solution was cast on a GOx-CDs membrane and the electrode was dried at 4 °C before use. In the detection of glucose, the GOx-CDs enzyme electrode was used as a working electrode, a carbon electrode as a counter electrode, and a saturated calomel electrode (SCE) as a reference electrode. CV measurement was performed using a three-electrode cell in different concentrations of O_2-saturated glucose solutions (0, 0.25, 0.5, 1, 2, and 3 mmol/L). For comparison, a GOx enzyme electrode was prepared by the same method.

2.6. Interference Test. The interference tests were carried out by CV measurement in 2 mmol/L O_2-saturated glucose (Glc) and the same concentrations of interfering substances, dopamine (DA), uric acid (UA), ascorbic acid (Vc), L-cysteine (Cys), and L-tyrosine (Tyr). The interference of these substances was assessed from the change of the reductive peak current compared with the GOx-CDs enzyme electrode in O_2-saturated 0.1 mol/L PBS (pH = 7.2).

3. RESULTS AND DISCUSSION

3.1. Synthesis and Structure of Chiral CDs. In this work, the chiral CDs were synthesized by two-step pyrolysis of organic molecules. As illustrated in Figure 1, first, citric acid

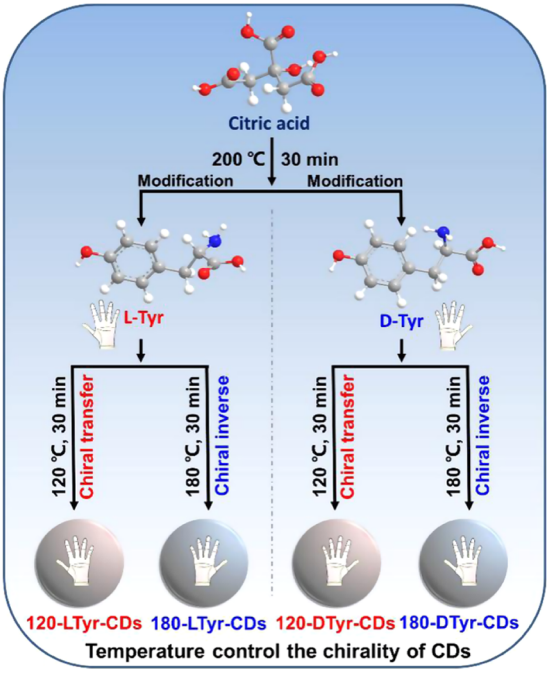

Figure 1. Schematic for controlled chiral transfer and inversion of CDs via a temperature-induced surface modification. At a low reaction temperature of 120 °C, due to the chiral transfer, the CDs have the same handedness of chirality as the chiral source, whereas, at 180 °C, the CDs have reversed handedness compared to the chiral source.

was carbonized at 200 °C for 30 min, and then L-/D-Try, as a chiral source, was added into the reaction system and reacted with the carbon core formed by carbonized citric acid at 120/180 °C for 30 min. After the surface modification, the chiral CDs (120-LTyr-CDs, 120-DTyr-CDs, 180-LTyr-CDs, and 180-DTyr-CDs) were finally obtained. The detailed synthetic process and purification steps are shown in Section 2. Notably, with this method, the controlled chiral transfer and inversion of CDs can be realized by adjusting the reaction temperature. When L-Tyr served as the chiral source, the 120-LTyr-CDs inherited the same handedness as the precursor at 120 °C, but 180-LTyr-CDs with the inverted chiral signal were obtained at a higher reaction temperature of 180 °C. Similarly, with D-Tyr as the chiral precursor, the symmetric enantiomers (120-DTyr-CDs and 180-DTyr-CDs) of 120-LTyr-CDs and 180-LTyr-CDs could be obtained at 120 and 180 °C, respectively.

In the following study, the morphological and structural characterizations of chiral CDs were analyzed. The chiral CDs (120-LTyr-CDs, 120-DTyr-CDs, 180-LTyr-CDs, and 180-DTyr-

https://dx.doi.org/10.1021/acsami.0c21949
ACS Appl. Mater. Interfaces 2021, 13, 5877−5886

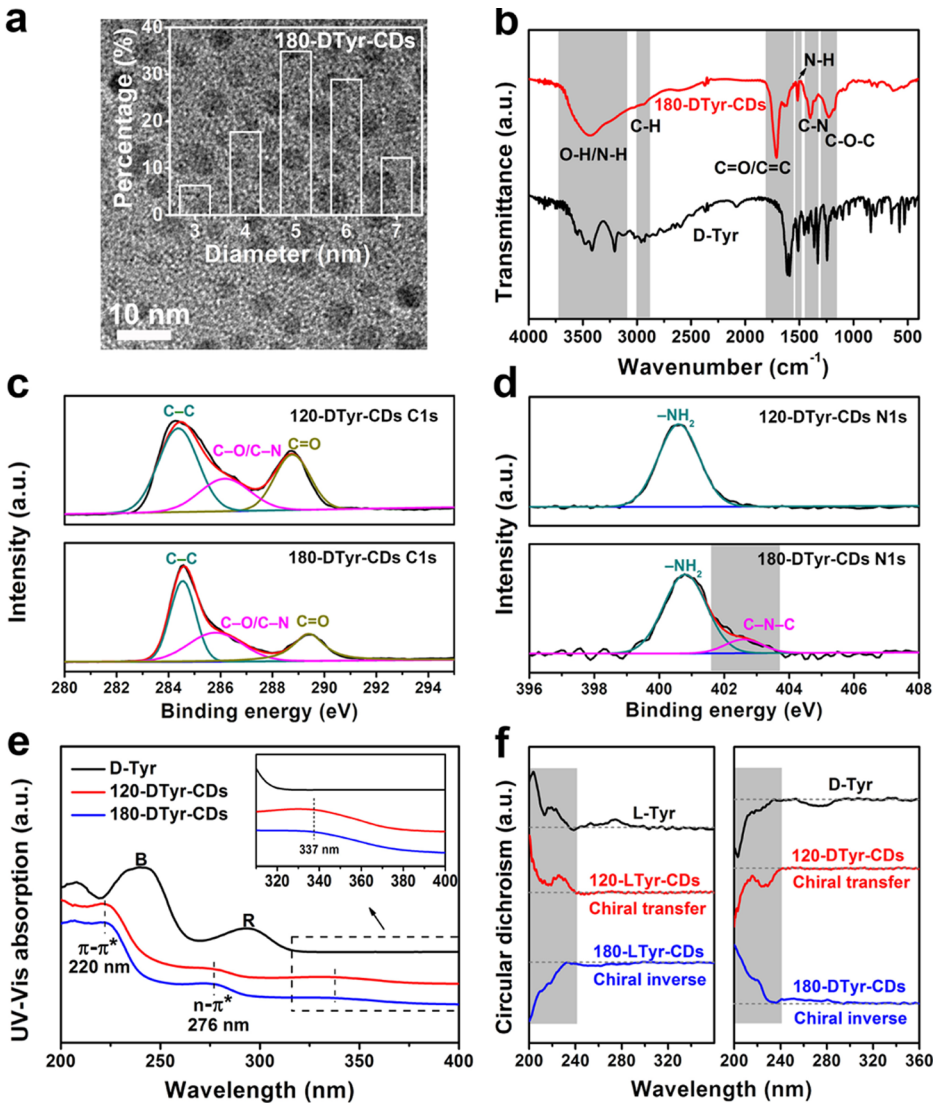

Figure 2. Characterization of chiral CDs. (a) TEM image and size distribution (inset) of 180-D-Tyr-CDs; (b) the FT-IR spectra of 180-D-Tyr-CDs (red line) and D-Tyr (black line); (c) the C 1s and (d) N 1s high-resolution XPS spectra of 120-D-Tyr-CDs and 180-D-Tyr-CDs; (e) the UV−vis absorption spectra of D-Tyr, 120-D-Tyr-CDs, and 180-D-Tyr-CDs; and (f) the circular dichroism spectra of L-Tyr (left, black line), 120-L-Tyr-CDs (left, red line), 180-L-Tyr-CDs (left, blue line), D-Tyr (right, black line), 120-D-Tyr-CDs (right, red line), and 180-D-Tyr-CDs (right, blue line).

CDs) had similar morphologies and structures, hence 180-D-Tyr-CDs are mainly discussed in the main text. First, the morphological characterization of CDs was studied by a transmission electron microscope (TEM). As shown in Figure S1a,b, the size distribution of carbonated citric acid ranged from 2 to 5 nm. When the carbon core was modified with Tyr, the chiral CDs had similar morphological features and their diameters increased to 3−7 nm (shown in Figures 2a and S1c−h). In addition, Fourier transform infrared (FT-IR) spectroscopy (Figures 2b and S2) was adopted for analyzing the composition of chiral CDs as well. The vibrational absorption signals of 180-D-Tyr-CDs were less than D-Tyr. With regard to the FT-IR spectrum of 180-D-Tyr-CDs, the stretching vibration signals of O−H/N−H at 3427 cm^{-1}, C−H at 2922 cm^{-1}, and C═O/C═C at 1710 cm^{-1} are shown, respectively.[36,37] Besides, the peaks located at 1519, 1398, and 1232 cm^{-1} could be assigned to the bending vibrations of N−H and the stretching vibration of C−N and C−O−C, respectively.[36,38] The FT-IR spectrum of 180-D-Tyr-CDs demonstrated that the amino acid L-/D-Tyr was successfully modified on the carbon core and the surface of CDs mainly possessed some hydrophilic functional groups, such as carboxyl, oxhydryl, and amidogen.

X-ray photoelectron spectroscopy (XPS) was adopted for further analyzing the structure and the composition characterization of the chiral CDs. The full-scan XPS spectrum (Figure S3d) shows that the 180-D-Tyr-CDs consisted of carbon, oxygen, and nitrogen elements and the atomic percentages for the above elements were 60.47, 34.26, and 5.27%, respectively. The C 1s spectrum of 180-D-Tyr-CDs, shown in the bottom of Figure 2c, could be divided into three surface components. The peaks located at 284.6, 285.8, and 289.4 eV corresponded to C−C, C−O/C−N, and C═O, respectively.[27,39] The N 1s spectrum of 180-D-Tyr-CDs, shown at the bottom of Figure 2d, could be divided into two peaks located at 400.8 and 402.6 eV. The first peak was assigned to $-NH_2$, whereas the last peak belonged to C−N−C.[33] However, in the N 1s high-resolution XPS spectra of these four chiral CDs, C−N−C could be found in the 180-L-Tyr-CDs (Figure S3d) and 180-D-Tyr-CDs (bottom of Figure 2e), whereas C−N−C was not present in

https://dx.doi.org/10.1021/acsami.0c21949
ACS Appl. Mater. Interfaces 2021, 13, 5877−5886

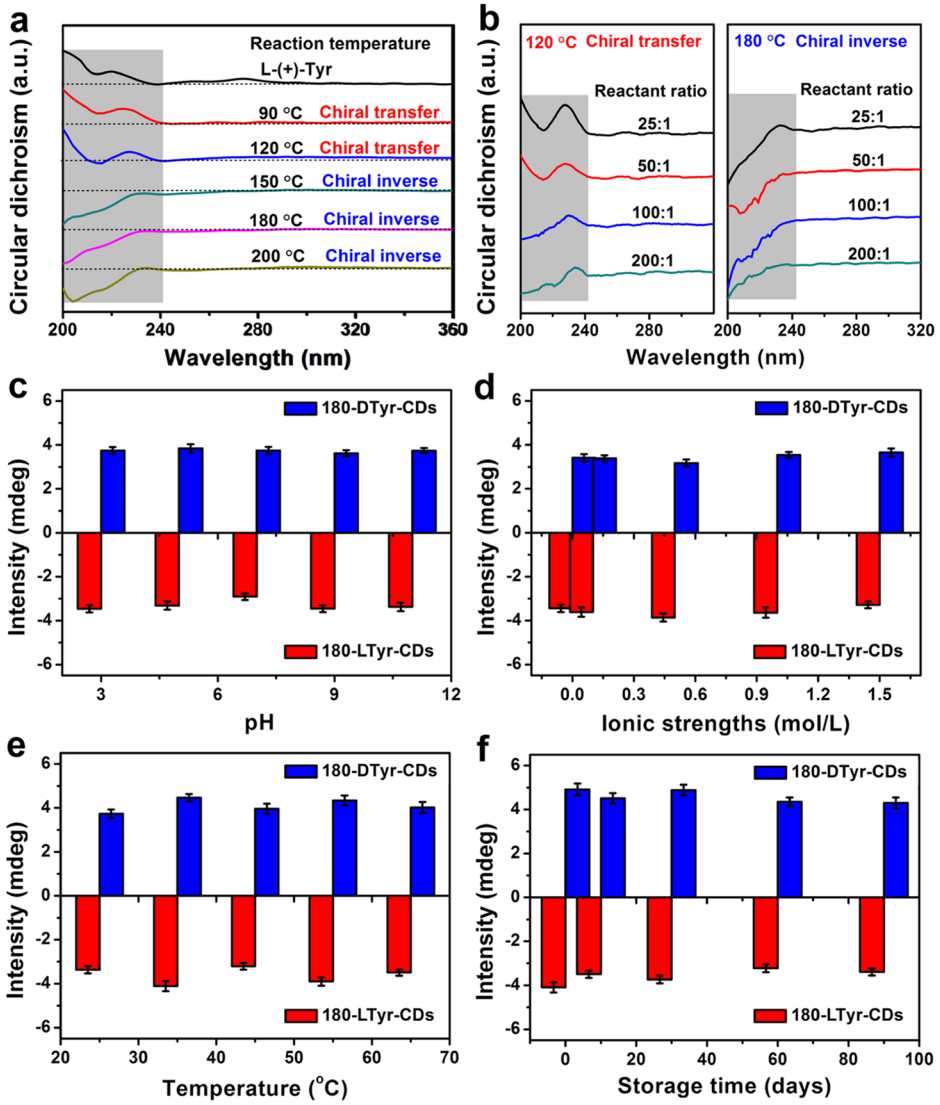

Figure 3. Handedness control and the stability of chiral CDs. (a) Circular dichroism spectra of CDs synthesized at different temperatures (90, 120, 150, 180, and 200 °C); (b) the circular dichroism spectra of CDs recorded at different ratios of citric acid and L-Tyr (25:1, 50:1, 100:1, and 200:1) at 120 and 180 °C; and the chiral stability of 180-LTyr-CDs and 180-DTyr-CDs at (c) different pH values (3.0−11.0), (d) different ionic strengths (0−1.5 mol/L NaCl), (e) different temperatures (25−95 °C), and (f) different storage times (0−90 days).

120-LTyr-CDs (Figure S4b) and 120-DTyr-CDs (top of Figure 2d). Hence, the new chemical bond of C−N−C at 402.6 eV may be due to the response for the change of the chiral CDs signal (180-LTyr-CDs and 180-DTyr-CDs). More information about TEM images, XPS, and FT-IR spectra of 120-LTyr-CDs, 120-DTyr-CDs, and 180-LTyr-CDs is provided and shown in Figures S1−S4. All those chiral CDs possessed similar size distribution, structure, and composition but different chiral optical properties and the bonding structure of nitrogen.

Next, the UV−vis absorption spectra and circular dichroism spectra of chiral CDs and Tyr in a water solution are shown in Figure 2e,f. The UV−vis absorption spectrum of D-Tyr (Figure 2e, black line) displayed two obvious peaks located at 240 and 292 nm, which corresponded to the B band and R band due to the electron transition of $\pi-\pi^*$ and $n-\pi^*$, respectively. For 120-DTyr-CDs and 180-DTyr-CDs (Figure 2e, red and blue lines), three absorption peaks at 220, 276, and 337 nm were observed. The first peak at 220 nm could be assigned to the $\pi-\pi^*$ electron transitions of the sp^2-hybridized carbon network.[40] The second peak at 276 nm could be attributed to the $n-\pi^*$electron transitions of C═O or C−N.[27,40] The trapping of excited-state energy by the surface states at 337 nm led to the emission at 451 nm (Figure S6).[27]

Then, we used circular dichroism spectra for characterizing the chirality of CDs. The difference in the absorption of left and right circularly polarized light could quantitatively analyze the handedness of CDs chirality.[41] The circular dichroism spectra of 120-LTyr-CDs (the left of Figure 2f, red line) and 120-DTyr-CDs (the right of Figure 2f, red line) revealed symmetric positive and positive/negative cotton effects at 227 nm, which inherited the same circular dichroism signal of L-Tyr (left of Figure 2f, black line) and D-Tyr (the right of Figure 2f, black line), respectively. In addition, the circular dichroism signals of 120-DTyr-CDs (the right of Figure 2f, red line) were in line with the UV absorption band (Figure 2e, red line). For 180-DTyr-CDs (right of Figure 2f, blue line), the handedness of chirality was opposite to D-Tyr, and they displayed two positive cotton effects at 220 and 252 nm and revealed a symmetric curve with 180-LTyr-CDs (the left of Figure 2f, blue line), displaying two negative cotton effects at 221 and 252 nm.

https://dx.doi.org/10.1021/acsami.0c21949
ACS Appl. Mater. Interfaces 2021, 13, 5877−5886

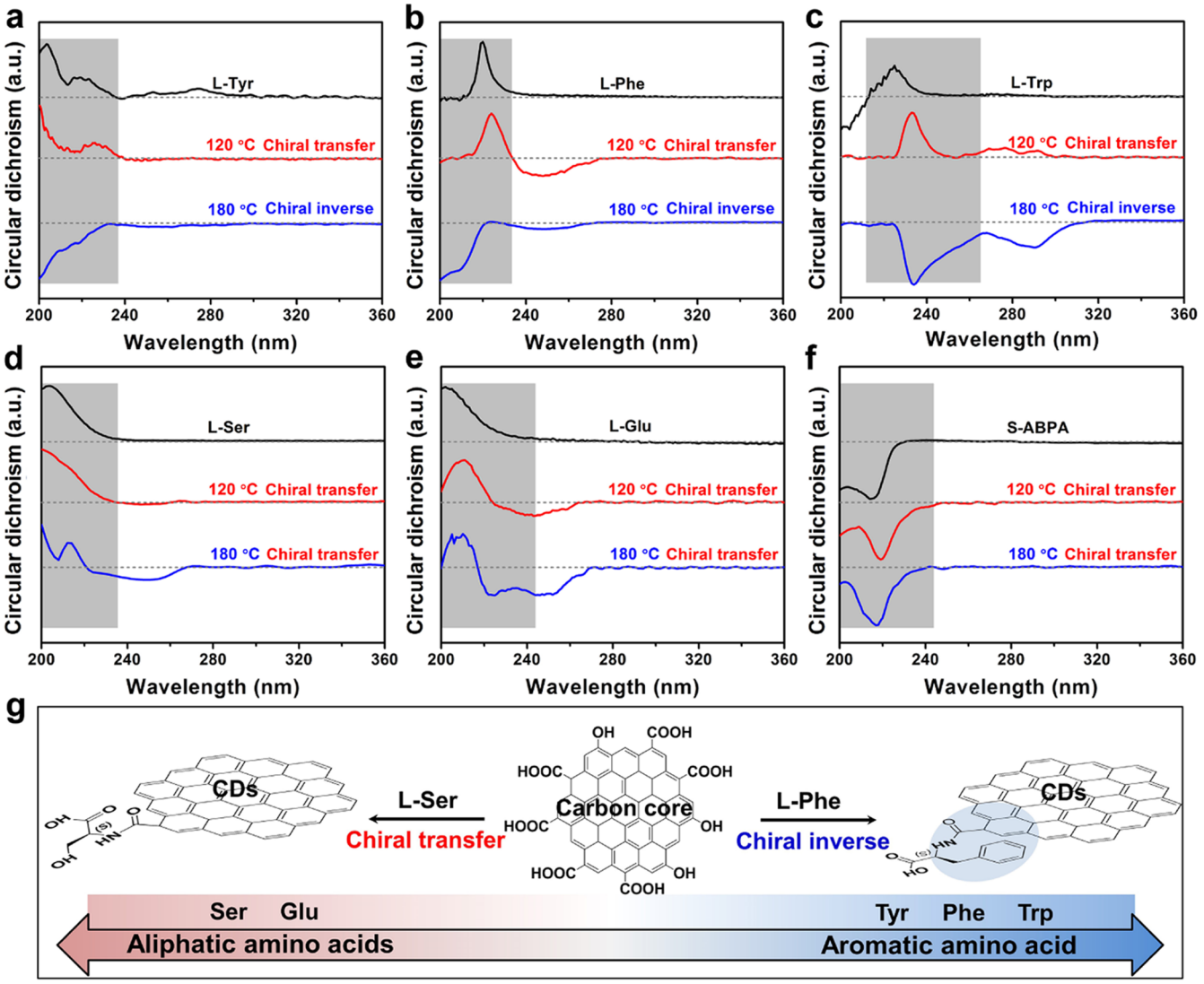

Figure 4. Possible synthesis mechanism of chiral CDs. The circular dichroism spectra of different chiral raw materials ((a) L-Tyr, (b) L-Phe, (c) L-Trp, (d) L-Ser, (e) L-Glu, and (f) (S)-(−)-ABPA) and the circular dichroism spectra of the corresponding chiral CDs prepared at 120 and 180 °C. (g) Schematic diagram of the synthesis mechanism of the chiral CDs.

The chiroptical asymmetry parameter (*g*-factor) was adopted as a fair standard for characterizing the chiroptical effects of CDs as well. As shown in Figure S7, the *g*-factor of the obtained chiral CDs is approximately 1×10^{-3}, which is higher than that of chiral CDs previously reported but still lower than that of many chiroplasmonic assemblies.[21,26,41] All of the above results suggested that the inversion of handedness was successfully retained from Tyr to CDs via temperature-induced surface modification.

3.2. Handedness Control of Chiral CDs. To investigate the reasons for the chiral formation of CDs, a series of contrast experiments were performed. In the first place, different temperatures (90, 120, 150, 180, and 200 °C) were used for the connection of carbonated citric acid and L-Tyr. Figure 3a shows that the circular dichroism spectra of CDs reacted at different temperatures. Compared with the chiral source (L-Tyr), when the connection temperature reached 150 °C, the chiral signals of CDs were inverse. Only the CDs that reacted below 120 °C inherited the same chiral signal as L-Tyr. Then, two temperatures (120 and 180 °C) were chosen for investigating the influence of the reactant ratio, and different reactant proportions (citric acid/L-Tyr, 25:1, 50:1, 100:1, and 200:1) were used. As shown in Figure 3b, even though few L-Tyr were added, the obtained CDs still possessed the inverse chiral signal to the chiral source at a temperature of 180 °C, whereas the handedness of the CDs maintains the circular dichroism absorption as the chiral source at 120 °C. In addition, the stability of the CDs handedness of circular dichroism was analyzed. The chiral signals of the characteristic peaks of chiral CDs (Figure S7, for 120-LTyr-CDs and 120-DTyr-CDs: 227 nm; 180-LTyr-CDs and 180-DTyr-CDs: 220 nm) at different pH values (3.0−11.0), different ionic strengths (0−1.5 mol/L NaCl), and different temperatures (25−95 °C), and different stabilization times (0−90 days) were monitored. As shown in Figures 3c−f and S8, the circular dichroism signal of the chiral CDs (120-LTyr-CDs, 120-DTyr-CDs, 180-LTyr-CDs, and 180-DTyr-CDs) was stable in the case of strong acidity, strong alkalinity, high ionic strength, and high temperature conditions, as well as at long-term storage (over 90 days).

It still remains a doubt that whether the high temperature would allow the transformation of the chiral signal of the raw

https://dx.doi.org/10.1021/acsami.0c21949
ACS Appl. Mater. Interfaces 2021, 13, 5877−5886

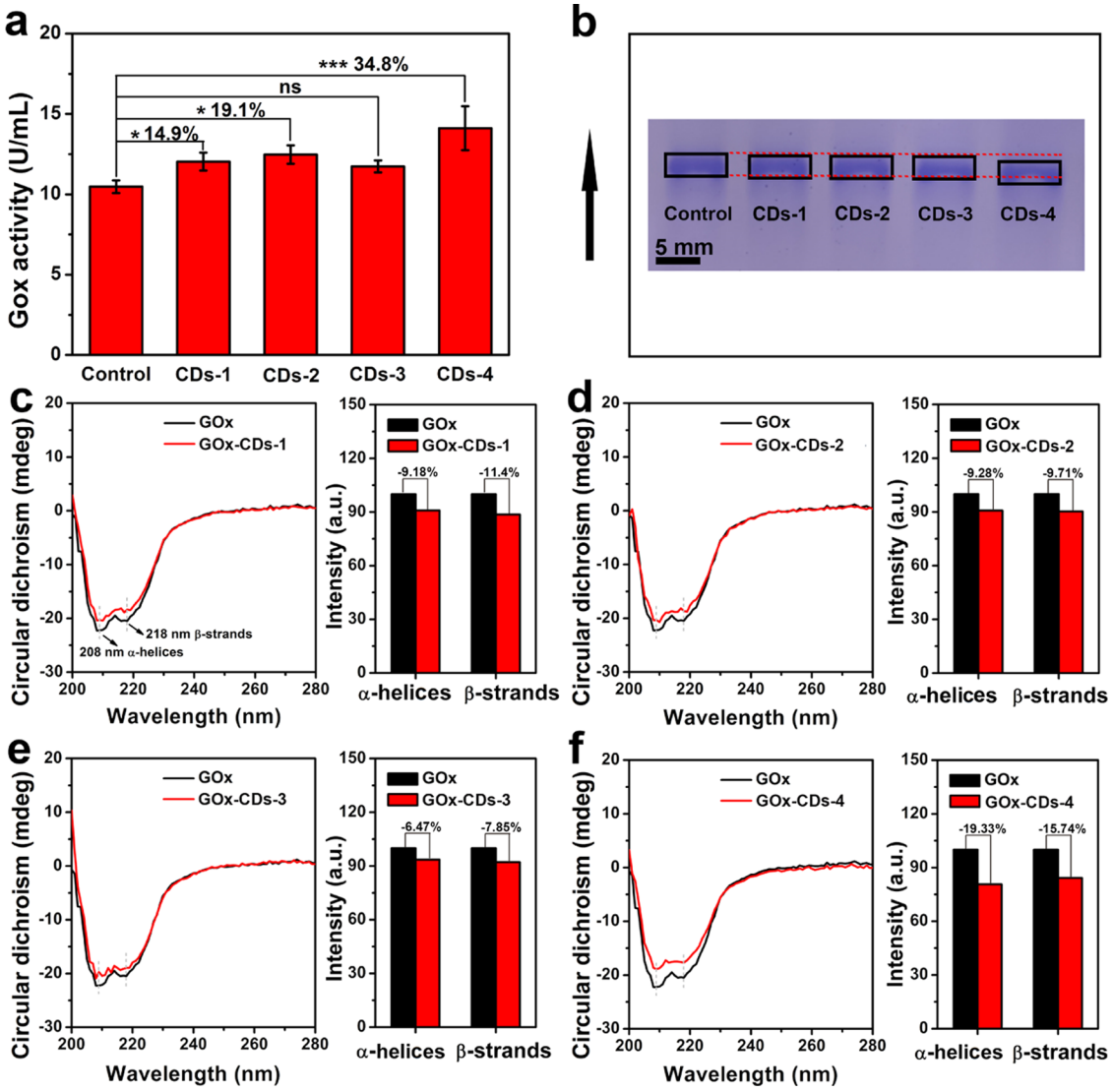

Figure 5. Effects of chiral CDs on GOx activity. (a) Enzymatic activity, (b) SDS-PAGE, and (c–f) circular dichroism spectra of GOx, GOx-CDs-1, GOx-CDs-2, GOx-CDs-3, and GOx-CDs-4, and the corresponding relative intensity of α-helices and β-strands (CDs/GOx = 1:3.75, mean ± SD, $^{*}P < 0.05$ and $^{***}P < 0.001$).

materials. Therefore, the independent carbon source (citric acid) and chiral source (Tyr) were treated by an oil bath of 200 and 180 °C for 30 min, respectively. As shown in Figure S9, the carbonated citric acid did not possess the chiral signal, while the chiral signal of L-Tyr was maintained, demonstrating that the inverse of the chiral signal of CDs was not derived from the carbonated citric acid or the chiral source but derived from their interaction. A hypothesis was proposed that the change of the handedness of CDs was due to the connection of carbonated citric acid and monomolecular L-Tyr. In the N 1s high-resolution XPS spectra of 180-DTyr-CDs (bottom of Figure 2d), a new chemical bond of C–N–C was found, demonstrating that L-Tyr may be linked to the carbonated citric acid via an amido bond. Thereafter, representative amino acids were chosen, such as simple aliphatic amino (Ser, Glu, Asp, and Cys) and aromatic amino acids (Phe and Trp), similar to Tyr. These amino acids reacted with carbonated citric acid at 120 and 180 °C for 30 min and their chiral signals were monitored, respectively. As shown in Figure 4a–f, when the reaction temperature was 120 °C, the chiral signals of all of the CDs (red line) were transferred by the chiral source (black line). However, at a reaction temperature of 180 °C, the circular dichroism signals of the CDs prepared from aromatic amino acids (Figure 4a–c, blue line) were opposite to the raw materials, whereas the chiral CDs derived from aliphatic amino acids (Figures S10 and 4d,e, blue line) maintained the cotton effects of the raw materials. It is worth noting that, compared with the chiral source, the disappearance of circular dichroism signals were due to the change of functional groups attached to the chiral center with the connection of amino acids (chiral source) and carbonized citric acid. The appearance of the new circular dichroism signals may likely be due to the formation of a new chiral center.[26] The handedness of the CDs discussed in this work, chiral transfer or reverse, is only for the inheritance of chiral raw materials. The newly generated chiral signal of CDs is not discussed specifically in this paper. For verifying that the inverse of the chiral signal was due to the connection between the amidogen of amino acid and the carboxyl of a carbon core, (S)-ABPA was used. Compared with the chemical structure of L-Phe, (S)-ABPA has one additional methylene (Figure S11). If the inverse of the CDs handedness was because of the esterification of aromatic amino acids and

https://dx.doi.org/10.1021/acsami.0c21949
ACS Appl. Mater. Interfaces 2021, 13, 5877–5886

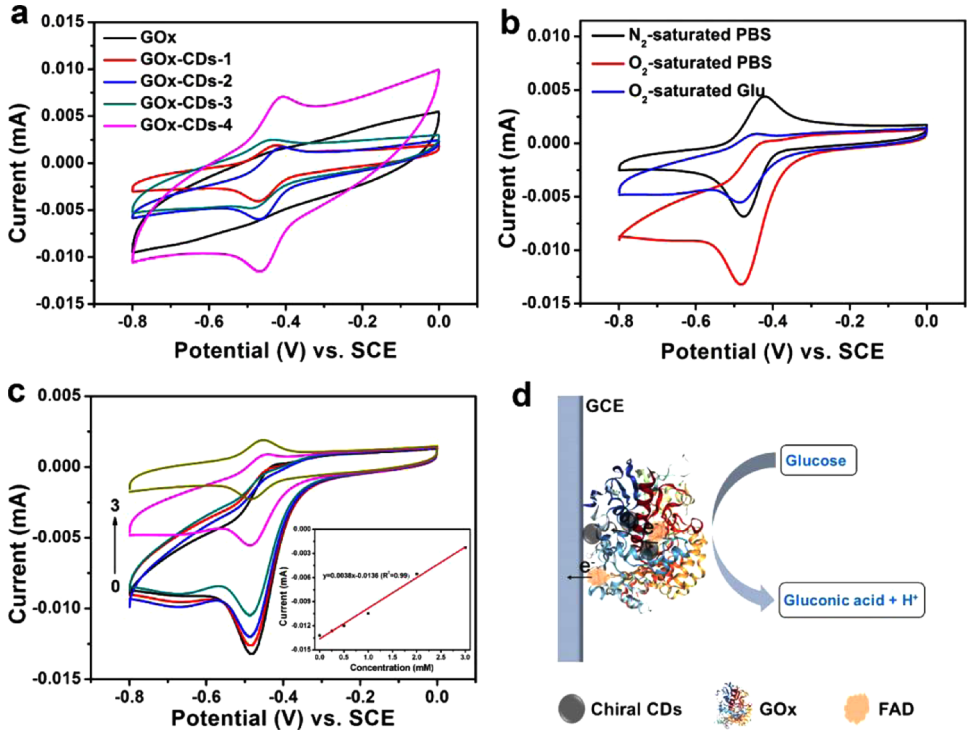

Figure 6. GOx-chiral CDs glucose sensor. (a) CVs of GOx (black line), GOx-CDs-1 (red line), GOx-CDs-2 (blue line), GOx-CDs-3 (green line), and GOx-DCDs-4 (purple line) in the N_2-saturated 0.1 mol/L PBS solution (pH = 7.2); (b) CVs of GOx-CDs-4 in the N_2-saturated 0.1 mol/L PBS solution (pH = 7.2, black line), O_2-saturated 0.1 mol/L PBS solution (pH = 7.2, red line), and O_2-saturated 2 mmol/L glucose solution (blue line); (c) CVs of GOx-CDs-4 in different concentrations of O_2-saturated glucose solutions (0, 0.25, 0.5, 1, 2, 3 mmol/L); and (d) schematic diagram of the GOx-CDs-4 glucose sensor. The scan rate is 100 mv/s.

carbon core rather than that of amidation, the addition of methylene in (S)-ABPA would not influence the inverse of handedness and the chiral signal of CDs synthesized from (S)-ABPA would inverse the handedness similar to the CDs obtained from L-Phe. As shown in Figure 4f, the (S)-ABPA-CDs had the same chiral signal as (S)-ABPA, demonstrating that the amidogen of the chiral source was the key factor in the formation of chiral CDs with an inverse chiral signal, and the connection of a carbon core and a chiral source was mainly via amidation at 180 °C.

Based on the above discussion, a possible synthesis mechanism for the formation of chiral CDs was suggested as follows. The carbon core with carboxyl groups was formed by carbonizing the citric acid in the first step of the synthesis. Then, as shown in Figure S12, the carbon core could be modified by a chiral source via amidation (type I) or esterification (type II and type III). For simple aliphatic amino acids, such as L-Ser, the chiral CDs with the same chiral signal compared with the chiral source were obtained for all of the three connective types. However, for an aromatic amino acid, L-Pen as an example, when the amido bond (type I) was formed, a rigid structure generated from the amide linkage to the aromatic nucleus of amino acid due to the conjugation of a π electron between the aromatic nucleus of amino acid and the carbon core, resulting in the warp of the configuration of L-Pen; and the CDs chiral signal was inverse compared with the chiral source. When the L-Pen is connected with the carbon core by esterification (type II), the rotatable ether bond between the surface of the carbon core and the L-Pen impeded the formation of a rigid structure and that connective type did not influence the chiral signal of CDs. Then, the chiral CDs with the transfer chiral signal obtained from (S)-(−)-ABPA verified the key factor of the amidogen of the chiral source and the effects of the rotatable single bone. The rigid structure could not be formed when the chain, from the carbon core to the chiral center of amino acid, existed as a rotatable bone. In the previous discussion, the chiral CDs derived from amino acids would maintain the handedness of the precursor at 120 °C. Furthermore, for making the reaction more complete at this temperature, the reaction time in the connection was prolonged and the reaction temperature was kept at 120 °C. As shown in Figure S13, although the reaction time extended to 90 min, the handedness of CDs remained the same as that of L-Tyr. This may be because amidation could not be carried out at 120 °C. The decomposition of ammonium carboxylate to amide is a reversible reaction. Higher temperature is beneficial for dehydration to form amide and move the equilibrium forward. Hence, the reaction at 120 °C could not connect the chiral source with the carbon core by the amido bond (type I) and the chiral CDs maintained the chiral signal of the raw material. To sum up, the handedness of CDs derived from amino acid could be inherited (transfer or reverse) via the amido bond between the amino acid and the carbonized citric acid at 180 °C. As shown in Figure 4g, for aliphatic amino acids (such as Ser and Glu), the handedness of CDs was transferred by the chiral source at a reaction temperature of 180 °C; for aromatic amino acids (such as Tyr, Phe, and Trp), the chiral CDs with the opposite chiral signal as the chiral source were obtained because of the warp of the configuration of the chiral source by the rigid structure generated by the amide bond and the conjugation of the π electron between the aromatic nucleus of the amino acid.

3.3. Effects of Chiral CDs on GOx Activity. Glucose oxidase (GOx) is an oxidase for specifically catalyzing glucose

https://dx.doi.org/10.1021/acsami.0c21949
ACS Appl. Mater. Interfaces 2021, 13, 5877−5886

to gluconic acid and it has been widely applied to biofuels and glucose biosensors.[42,43] In the following experiments, chiral CDs were used for tuning the GOx catalytic activity, and the chiral effects of CDs on GOx activity were investigated. As shown in Figure 5a, the chiral CDs could impact the enzymatic activity of GOx. The 120-LTyr-CDs, 120-DTyr-CDs, and 180-LTyr-CDs (hereinafter called CDs-1, CDs-2, and CDs-3 for short) caused only a slight increase in the GOx activity, whereas the 180-DTyr-CDs (CDs-4) significantly increased GOx activity (+34.8%). Further, the combination of chiral CDs with GOx was studied by a sodium dodecyl sulfate-polyacrylamide gel electrophoresis (SDS-PAGE) test. As shown in Figure 5b, the SDS-PAGE test demonstrated that the chiral CDs were combined with GOx successfully, and the shorter displacement distance of GOx-CDs-4 proved that the GOx-CDs-4 combined more effectively with GOx than GOx-CDs-1, GOx-CDs-2, and GOx-CDs-3. Figure 5c–f shows the change of the secondary structure of GOx-CDs-1, GOx-CDs-2, GOx-CDs-3, and GOx-CDs-4 compared with free GOx. The circular dichroism spectrum of GOx had the highest peak intensity at 208 nm (α-helix) and 218 nm (β-helices), while the spectra of chiral CDs-treated GOx possessed lower intensity of α-helix and β-helices. The GOx-180-DTyr-CDs with the lowest peak intensity suggested that the 180-DTyr-CDs strongly loose the GOx structure and expose the active sites, leading to the high catalytic activity of GOx-180-DTyr-CDs. For analyzing the combination pattern of GOx and chiral CDs, the PL spectrum was adopted. Figure S14 shows the PL spectra of GOx, 180-DTyr-CDs, and GOx-180-DTyr-CDs. The location of the fluorescence peak of GOx-CDs did not change compared with the GOx and CDs, so that the chiral CDs could likely be combined with GOx by adsorption. They would be adsorbed on the surface or the inside of the GOx.

Further, the GOx enzyme sensor was used for further verifying the enzyme regulation ability of chiral CDs and the chiral effects of CDs on the performance of the biosensor. A GOx-based direct electrochemical biosensor was designed and a GOx-CDs-modified GCE electrode was fabricated. One free GOx GCE electrode and four GOx-chiral CDs-modified GCE electrodes were fabricated, namely, free GOx, GOx-CDs-1, GOx-CDs-2, GOx-CDs-3, and GOx-CDs-4 electrodes. Cyclic voltammetry (CV) measurement was used for evaluating the electrochemical performances of these GOx-based enzyme biosensors. Figure 6a shows the CVs of GOx (black line), GOx-CDs-1 (red line), GOx-CDs-2 (blue line), GOx-CDs-3 (green line), and GOx-CDs-4 (purple line) in a N_2-saturated 0.1 mol/L PBS solution (pH = 7.2). No redox peaks were observed at the free GOx, whereas a pair of quasi-reversible redox peaks were detected at GOx-CDs-1, GOx-CDs-2, GOx-CDs-3, and GOx-CDs-4; GOx-CDs-4 had the superior peak current with the reduction peak potential of −0.47 V and peak-to-peak separation (ΔE_p) of 58 mV. The redox reaction of a flavin adenine dinucleotide (FAD, the redox-active center of GOx) could not be carried out in the free GOx electrode, which demonstrated that the free GOx casted in GCE could not conduct electricity directly due to the spatial position of the redox active center wrapped by a peptide chain polymer and carbohydrate.[44,45] However, the chiral CDs could be used as a substrate attached with GOx and conduct the electron transfer of GOx directly. Then, the CVs of the GOx-CDs-4 in a N_2-saturated 0.1 mol/L PBS solution (pH = 7.2) at different scan rates (50–500 mV/s) were detected. As shown in Figure S15, the intensity of redox peaks increased with the increasing scan rate. In addition, the peak currents of a cathode and an anode were similar ($i_{pa}/i_{pc} \approx 1$) and the potential of redox peaks only shifted slightly (ΔE_p = 58–62 mV), indicating that the GOx-180-DTyr-CDs had the typical property of a surface electrochemical behavior with the quasi-reversible reaction.

Due to the better electrochemical performances of GOx-CDs-4, its electrocatalytic activity was also measured as a glucose biosensor. Figure 6b shows the CVs of GOx-CDs-4 in a N_2-saturated 0.1 mol/L PBS solution (pH = 7.2, black line), O_2-saturated 0.1 mol/L PBS solution (pH = 7.2, red line), and O_2-saturated 2 mmol/L glucose solution (blue line). In a N_2-saturated 0.1 mol/L PBS solution, the GOx-CDs-4 displayed a pair of symmetrical redox peaks, demonstrating that a reversible process (FAD_{ox}/FAD_{red}) was carried out on the surface of a GOx-CDs-4 electrode. In an oxygen atmosphere, the reduced FAD of GOx-CDs-4 would be oxidized by O_2 with an increase in i_{pc} and decrease in i_{pa}. With the addition of 2 mmol/L glucose, the GOx-CDs-4 catalyzed the formation of glucose into gluconic acid and the oxydic FAD would be reduced with a decrease in i_{pc}compared with the condition of an O_2-saturated 0.1 mol/L PBS solution. Then, the response of a GOx-CDs-4 glucose sensor toward different concentrations of glucose was studied as well. As shown in Figure 6c, i_{pc} was proportional to the glucose concentration. The relation curve of i_{pc} of GOx-CDs-4 and the glucose concentration is shown in the inset of Figure 6c. They had a linear relation in the range of 0.25–3 mmol/L glucose, indicating that the GOx-CDs-4-modified GCE could serve as a sensitive glucose biosensor. Anti-interference ability is an important factor for a biosensor. Next, the interference tests were carried out by CV measurement in the presence of 2 mmol/L glucose (Glc) and the same concentration of an interfering substances, such as DA, UA, Vc, Cys, and Tyr. As shown in Figure S16, the GOx-CDs-4-modified GCE could only recognize that the glucose, and the interfering substances (DA, UA, Vc, Cys, and Tyr) did not influence the response of GOx-CDs-4.

The schematic catalytic mechanism of a GOx-chiral CDs glucose sensor is shown in Figure 6d. On the surface of an electrode, the addition of chiral CDs loses the GOx structure and the redox center (FAD) wrapped by a peptide chain was exposed so that the FAD was close to the surface of the electrode and realized the direct electron transfer. Besides, the CDs could also play the role of electron conduction. The CDs attached to GOx could convey the electron of FAD, which was far away from the surface of the electrode. In the enzyme layer, GOx with high specificity could identify glucose and catalyze the formation of glucose into gluconic acid and a proton. Thus, the chiral CDs could serve as a new substrate for enzyme regulation and direct electrochemistry of GOx, and the GOx-CDs-4 have a superior electrocatalytic activity.

4. CONCLUSIONS

In summary, we regulated the handedness of CDs by adjusting the temperature of thermal polymerization from citric acid and chiral amino acids. For aliphatic amino acids (such as Ser, Glu, Asp, and Cys), the handedness of CDs was transferred by a chiral source. For aromatic amino acids (such as Tyr, Phe, and Trp), the chiral CDs could inherit the same chiral signal as the chiral raw material at 120 °C, whereas the chiral CDs with the inverted signal could be obtained at higher temperatures (above 150 °C). At a high reaction temperature, the chiral source was beneficial for modifying the carbon core via amidation. Then, a rigid structure was generated due to the

https://dx.doi.org/10.1021/acsami.0c21949
ACS Appl. Mater. Interfaces 2021, 13, 5877–5886

conjugation of a π electron between an aromatic nucleus of amino acid and a carbon core, resulting in the warp of the configuration of aromatic amino acids and the inverse circular dichroism absorption of CDs compared with the chiral source. The obtained chiral CDs were further used to design and fabricate a sensitive GOx-chiral CDs glucose sensor by tuning the GOx catalytic activity. This work provides a new way of regulating the handedness of CDs and develops diverse chiral carbon nanomaterials for biological applications.

■ ASSOCIATED CONTENT

Supporting Information

The Supporting Information is available free of charge at https://pubs.acs.org/doi/10.1021/acsami.0c21949.

Material characterization, the experimental procedure for the circular dichroism measurement of GOx-CDs hybrids, sodium dodecyl sulfate-polyacrylamide gel electrophoresis, statistical analysis, the molecular formula of chiral source; supplementary data of chiral CDs, the possible chemical reaction of the synthesis of chiral CDs, and the interference test (PDF)

■ AUTHOR INFORMATION

Corresponding Authors

Yang Liu − *Institute of Functional Nano & Soft Materials (FUNSOM), Jiangsu Key Laboratory for Carbon-Based Functional Materials & Devices, Soochow University, Suzhou 215123, Jiangsu, China*; Email: yangl@suda.edu.cn

Hui Huang − *Institute of Functional Nano & Soft Materials (FUNSOM), Jiangsu Key Laboratory for Carbon-Based Functional Materials & Devices, Soochow University, Suzhou 215123, Jiangsu, China*; orcid.org/0000-0002-9053-9426; Email: hhuang0618@suda.edu.cn

Fang Lu − *School of Life Sciences, Beijing University of Chinese Medicine, Beijing 100029, China*; Email: lufang@bucm.edu.cn

Zhenhui Kang − *Institute of Functional Nano & Soft Materials (FUNSOM), Jiangsu Key Laboratory for Carbon-Based Functional Materials & Devices, Soochow University, Suzhou 215123, Jiangsu, China; Macau Institute of Materials Science and Engineering, Macau University of Science and Technology, Taipa 999078, Macau SAR, China*; orcid.org/0000-0001-6989-5840; Email: zhkang@suda.edu.cn

Authors

Mengling Zhang − *Institute of Functional Nano & Soft Materials (FUNSOM), Jiangsu Key Laboratory for Carbon-Based Functional Materials & Devices, Soochow University, Suzhou 215123, Jiangsu, China*

Yurong Ma − *Institute of Functional Nano & Soft Materials (FUNSOM), Jiangsu Key Laboratory for Carbon-Based Functional Materials & Devices, Soochow University, Suzhou 215123, Jiangsu, China*

Huibo Wang − *Institute of Functional Nano & Soft Materials (FUNSOM), Jiangsu Key Laboratory for Carbon-Based Functional Materials & Devices, Soochow University, Suzhou 215123, Jiangsu, China*

Bo Wang − *Institute of Functional Nano & Soft Materials (FUNSOM), Jiangsu Key Laboratory for Carbon-Based Functional Materials & Devices, Soochow University, Suzhou 215123, Jiangsu, China*

Yunjie Zhou − *Institute of Functional Nano & Soft Materials (FUNSOM), Jiangsu Key Laboratory for Carbon-Based Functional Materials & Devices, Soochow University, Suzhou 215123, Jiangsu, China*

Mingwang Shao − *Institute of Functional Nano & Soft Materials (FUNSOM), Jiangsu Key Laboratory for Carbon-Based Functional Materials & Devices, Soochow University, Suzhou 215123, Jiangsu, China*; orcid.org/0000-0002-4220-463X

Complete contact information is available at: https://pubs.acs.org/10.1021/acsami.0c21949

Author Contributions

This manuscript was written through the contributions of all authors. All authors have given approval to the final version of the manuscript.

Notes

The authors declare no competing financial interest.

■ ACKNOWLEDGMENTS

This work was supported by the National MCF Energy R&D Program (2018YFE0306105), the National Key Research and Development Project of China (2020YFA0406104), the Innovative Research Group Project of the National Natural Science Foundation of China (51821002), the National Natural Science Foundation of China (51725204, 21771132, 51972216, and 52041202), the Natural Science Foundation of Jiangsu Province (BK20190041), the Key-Area Research and Development Program of Guangdong Province (2019B010933001), the Collaborative Innovation Center of Suzhou Nano Science & Technology, the Priority Academic Program Development of Jiangsu Higher Education Institutions (PAPD), and the 111 Project.

■ REFERENCES

(1) Han, X.; Yuan, C.; Hou, B.; Liu, L.; Li, H.; Liu, Y.; Cui, Y. Chiral Covalent Organic Frameworks: Design, Synthesis and Property. *Chem. Soc. Rev.* **2020**, *49*, 6248−6272.

(2) Phipps, R. J.; Hamilton, G. L.; Toste, F. D. The Progression of Chiral Anions from Concepts to Applications in Asymmetric Catalysis. *Nat. Chem.* **2012**, *4*, 603−614.

(3) Zhao, X.; Zang, S. Q.; Chen, X. Stereospecific Interactions between Chiral Inorganic Nanomaterials and Biological Systems. *Chem. Soc. Rev.* **2020**, *49*, 2481−2503.

(4) Han, C.; Li, H. Chiral Recognition of Amino Acids Based on Cyclodextrin-Capped Quantum Dots. *Small* **2008**, *4*, 1344−1350.

(5) Wang, W.; Hao, C.; Sun, M.; Xu, L.; Wu, X.; Xu, C.; Kuang, H. Peptide Mediated Chiral Inorganic Nanomaterials for Combating Gram-Negative Bacteria. *Adv. Funct. Mater.* **2018**, *28*, No. 1805112.

(6) Martynenko, I. V.; Kuznetsova, V. A.; Litvinov, I. K.; Orlova, A. O.; Maslov, V. G.; Fedorov, A. V.; Dubavik, A.; Purcell-Milton, F.; Gun'ko, Y. K.; Baranov, A. V. Enantioselective Cellular Uptake of Chiral Semiconductor Nanocrystalsd. *Nanotechnology* **2016**, *27*, No. 075102.

(7) Wang, H. S.; Wei, J. P. Emerging Enantiomeric Resolution Materials with Homochiral Nano-Fabrications. *Nanoscale* **2015**, *7*, 11815−11832.

(8) Chen, C.; Shi, H.; Zhao, G. Chiral Recognition and Enantioselective Photoelectrochemical Oxidation toward Amino Acids on Single-Crystalline ZnO. *J. Phys. Chem. C* **2014**, *118*, 12041−12049.

(9) Sang, Y.; Han, J.; Zhao, T.; Duan, P.; Liu, M. Circularly Polarized Luminescence in Nanoassemblies: Generation, Amplification, and Application. *Adv. Mater.* **2019**, *32*, No. 1900110.

(10) Ben Dor, O.; Morali, N.; Yochelis, S.; Baczewski, L. T.; Paltiel, Y. Local Light-Induced Magnetization Using Nanodots and Chiral Molecules. *Nano Lett.* **2014**, *14*, 6042−6049.
(11) Milton, F. P.; Govan, J.; Mukhina, M. V.; Gun'ko, Y. K. The Chiral Nano-World: Chiroptically Active Quantum Nanostructures. *Nanoscale Horiz.* **2016**, *1*, 14−26.
(12) Schaaff, T. G.; Knight, G.; Shafigullin, M. N.; Borkman, R. F.; Whetten, R. L. Isolation and Selected Properties of a 10.4 kDa Gold: Glutathione Cluster Compound. *J. Phys. Chem. B* **1998**, *102*, 10643−10646.
(13) Lee, H. E.; Ahn, H. Y.; Mun, J.; Lee, Y. Y.; Kim, M.; Cho, N. H.; Chang, K.; Kim, W. S.; Rho, J.; Nam, K. T. Amino-Acid- and Peptide-Directed Synthesis of Chiral Plasmonic Gold Nanoparticles. *Nature* **2018**, *556*, 360−365.
(14) Huang, P.; Pandoli, O.; Wang, X.; Wang, Z.; Li, Z.; Zhang, C.; Chen, F.; Lin, J.; Cui, D.; Chen, X. Chiral Guanosine 5′-Monophosphate-Capped Gold Nanoflowers: Controllable Synthesis, Characterization, Surface-Enhanced Raman Scattering Activity, Cellular Imaging and Photothermal Therapy. *Nano Res.* **2012**, *5*, 630−639.
(15) Jin, X.; Jiang, J.; Liu, M. Reversible Plasmonic Circular Dichroism via Hybrid Supramolecular Gelation of Achiral Gold Nanorods. *ACS Nano* **2016**, *10*, 11179−11186.
(16) Kuzyk, A.; Urban, M. J.; Idili, A.; Ricci, F.; Liu, N. Selective Control of Reconfigurable Chiral Plasmonic Metamolecules. *Sci. Adv.* **2017**, *3*, No. e1602803.
(17) Mukhina, M. V.; Maslov, V. G.; Baranov, A. V.; Fedorov, A. V.; Orlova, A. O.; Purcell-Milton, F.; Govan, J.; Gun'ko, Y. K. Intrinsic CD of CdSe/ZnS Quantum Dots and Quantum Rods. *Nano Lett.* **2015**, *15*, 2844−2851.
(18) Ben-Moshe, A.; Wolf, S. G.; Bar Sadan, M.; Houben, L.; Fan, Z.; Govorov, A. O.; Markovich, G. Enantioselective Control of Lattice and Shape Chirality in Inorganic Nanostructures Using Chiral Biomolecules. *Nat. Commun.* **2014**, *5*, No. 4302.
(19) Yeom, J.; Yeom, B.; Chan, H.; Smith, K. W.; Dominguez-Medina, S.; Bahng, J. H.; Zhao, G.; Chang, W. S.; Chang, S. J.; Chuvilin, A.; Melnikau, D.; Rogach, A. L.; Zhang, P.; Link, S.; Král, P.; Kotov, N. Chiral Templating of Self-Assembling Nanostructures by Circularly Polarized Light. *Nat. Mater.* **2015**, *14*, 66−72.
(20) Roushan, P.; Neill, C.; Megrant, A.; Chen, Y.; Babbush, R.; Barends, R.; Campbell, B.; Chen, Z.; Chiaro, B.; Dunsworth, A.; Fowler, A.; Jeffrey, E.; Kelly, J.; Lucero, E.; Mutus, J.; O'Malley, P. J. J.; Neeley, M.; Quintana, C.; Sank, D.; Vainsencher, A.; Wenner, J.; White, T.; Kapit, E.; Neven, H.; Martinis, J. Chiral Ground-State Currents of Interacting Photons in a Synthetic Magnetic Field. *Nat. Phys.* **2017**, *13*, 146−151.
(21) Zhang, S.; Zhou, J.; Park, Y. S.; Rho, J.; Singh, R.; Nam, S.; Azad, A. K.; Chen, H. T.; Yin, X.; Taylor, A. J.; Zhang, X. Photoinduced Handedness Switching in Terahertz Chiral Metamolecules. *Nat. Commun.* **2012**, *3*, No. 942.
(22) Yoon, G.; Kim, I.; So, S.; Mun, J.; Kim, M.; Rho, J. Fabrication of Three-dimensional Suspended, Interlayered and Hierarchical Nanostructures by Accuracy-improved Electron Beam Lithography Overlay. *Sci. Rep.* **2017**, *7*, No. 6668.
(23) Du, J.; Xu, N.; Fan, J.; Sun, W.; Peng, X. Carbon Dots for In Vivo Bioimaging and Theranostics. *Small* **2019**, *15*, No. 1805087.
(24) Hu, C.; Li, M.; Qiu, J.; Sun, Y. P. Design and Fabrication of Carbon Dots for Energy Conversion and Storage. *Chem. Soc. Rev.* **2019**, *48*, 2315−2337.
(25) Liu, M. L.; Chen, B. B.; Li, C. M.; Huang, C. Z. Carbon Dots: Synthesis, Formation Mechanism, Fluorescence Origin and Sensing Applications. *Green Chem.* **2019**, *21*, 449−471.
(26) Suzuki, N.; Wang, Y.; Elvati, P.; Qu, Z. B.; Kim, K.; Jiang, S.; Baumeister, E.; Lee, J.; Yeom, B.; Bahng, J. H.; Lee, J.; Violi, A.; Kotov, N. A. Chiral Graphene Quantum Dots. *ACS Nano* **2016**, *10*, 1744−1755.
(27) Li, F.; Li, Y.; Yang, X.; Han, X.; Jiao, Y.; Wei, T.; Yang, D.; Xu, H.; Nie, G. Highly Fluorescent Chiral N-S-Doped Carbon Dots from Cysteine: Affecting Cellular Energy Metabolism. *Angew. Chem., Int. Ed.* **2018**, *57*, 2377−2382.
(28) Li, R. S.; Gao, P. F.; Zhang, H. Z.; Zheng, L. L.; Li, C. M.; Wang, J.; Li, Y. F.; Liu, F.; Li, N.; Huang, C. Z. Chiral Nanoprobes for Targeting and Long-term Imaging of the Golgi Apparatus. *Chem. Sci.* **2017**, *8*, 6829−6835.
(29) Xin, Q.; Liu, Q.; Geng, L.; Fang, Q.; Gong, J. R. Chiral Nanoparticle as a New Efficient Antimicrobial Nanoagent. *Adv. Healthcare Mater.* **2017**, *6*, No. 1601011.
(30) Zhang, M.; Hu, L.; Wang, H.; Song, Y.; Liu, Y.; Li, H.; Shao, M.; Huang, H.; Kang, Z. One-Step Hydrothermal Synthesis of Chiral Carbon Dots and Their Effects on Mung Bean Plant Growth. *Nanoscale* **2018**, *10*, 12734−12742.
(31) Zhang, M.; Wang, H.; Wang, B.; Ma, Y.; Huang, H.; Liu, Y.; Shao, M.; Yao, B.; Kang, Z. Maltase Decorated by Chiral Carbon Dots with Inhibited Enzyme Activity for Glucose Level Control. *Small* **2019**, *15*, No. 1901512.
(32) Hu, L.; Li, H.; Liu, C.; Song, Y.; Zhang, M.; Huang, H.; Liu, Y.; Kang, Z. Chiral Evolution of Carbon Dots and the Tuning of Laccase Activity. *Nanoscale* **2018**, *10*, 2333−2340.
(33) Đorđević, L.; Arcudi, F.; D'Urso, A.; Cacioppo, M.; Micali, N.; Buergi, T.; Purrello, R.; Prato, M. Design Principles of Chiral Carbon Nanodots Help Convey Chirality from Molecular to Nanoscale Level. *Nat. Commun.* **2018**, *9*, No. 3442.
(34) Li, F.; Li, S.; Guo, X.; Dong, Y.; Yao, C.; Liu, Y.; Song, Y.; Tan, X.; Gao, L.; Yang, D. Chiral Carbon Dots Mimicking Topoisomerase I To Mediate the Topological Rearrangement of Supercoiled DNA Enantioselectively. *Angew. Chem., Int. Ed.* **2020**, *59*, 11087−11092.
(35) Vázquez-Nakagawa, M.; Rodriguez-Perez, L.; Herranz, M. A.; Martin, N. Chirality Transfer from Graphene Quantum Dots. *Chem. Commun.* **2016**, *52*, 665−668.
(36) Li, D.; Li, W.; Zhang, H.; Zhang, X.; Zhuang, J.; Liu, Y.; Hu, C.; Lei, B. Far-Red Carbon Dots as Efficient Light-Harvesting Agents for Enhanced Photosynthesis. *ACS Appl. Mater. Interfaces* **2020**, *12*, 21009−21019.
(37) Xue, R.; Fu, L.; Dong, S.; Yang, H.; Zhou, D. Promoting Chlorella Photosynthesis and Bioresource Production Using Directionally Prepared Carbon Dots with Tunable Emission. *J. Colloid Interface Sci.* **2020**, *569*, 195−203.
(38) Li, H.; Huang, J.; Liu, Y.; Lu, F.; Zhong, J.; Wang, Y.; Li, S.; Lifshitz, Y.; Lee, S.-T.; Kang, Z. Enhanced RuBisCO Activity and Promoted Dicotyledons Growth with Degradable Carbon Dots. *Nano Res.* **2019**, *12*, 1585−1593.
(39) Zhang, M.; Su, R.; Zhong, J.; Fei, L.; Cai, W.; Guan, Q.; Li, W.; Li, N.; Chen, Y.; Cai, L.; Xu, Q. Red/Orange Dual-Emissive Carbon Dots for pH Sensing and Cell Imaging. *Nano Res.* **2019**, *12*, 815−821.
(40) Li, W.; Wu, S.; Zhang, H.; Zhang, X.; Zhuang, J.; Hu, C.; Liu, Y.; Lei, B.; Ma, L.; Wang, X. Enhanced Biological Photosynthetic Efficiency Using Light-Harvesting Engineering with Dual-Emissive Carbon Dots. *Adv. Funct. Mater.* **2018**, *28*, No. 1804004.
(41) Mun, J.; Kim, M.; Yang, Y.; Badloe, T.; Ni, J.; Chen, Y.; Qiu, C. W.; Rho, J. Electromagnetic Chirality: from Fundamentals to Nontraditional Chiroptical Phenomena. *Light: Sci. Appl.* **2020**, *9*, No. 139.
(42) Fu, L. H.; Qi, C.; Hu, Y. R.; Lin, J.; Huang, P. Glucose Oxidase-Instructed Multimodal Synergistic Cancer Therapy. *Adv. Mater.* **2019**, *31*, No. 1808325.
(43) Liu, Y.; Yu, D.; Zeng, C.; Miao, Z.; Dai, L. Biocompatible Graphene Oxide-Based Glucose Biosensors. *Langmuir* **2010**, *26*, 6158−6160.
(44) Razmi, H.; Mohammad-Rezaei, R. Graphene Quantum Dots as a New Substrate for Immobilization and Direct Electrochemistry of Glucose Oxidase: Application to Sensitive Glucose Determination. *Biosens. Bioelectron.* **2013**, *41*, 498−504.
(45) Zhai, D.; Liu, B.; Shi, Y.; Pan, L.; Wang, Y.; Li, W.; Zhang, R.; Yu, G. Highly Sensitive Glucose Sensor Based on Pt Nanoparticle/Polyaniline Hydrogel Heterostructures. *ACS Nano* **2013**, *7*, 3540−3546.

https://dx.doi.org/10.1021/acsami.0c21949
ACS Appl. Mater. Interfaces 2021, 13, 5877−5886